STEP UP IN IMAGE DEHAZING USING WAVELET DECOMPOSITION & GUIDED FILTERS

A PROJECT REPORT

Submitted by

HARPREET KAUR

2K13/SPD/25

in partial fulfillment for the award of the degree of

MASTER OF TECHNOLOGY

in

SIGNAL PROCESSING AND DIGITAL DESIGN

under the supervision of

DR. SUDIPTA MAJUMDAR

ASSISTANT PROFESSOR

DEPARTMENT OF

ELECTRONICS & COMMUNICATION ENGINEERING

DELHI TECHNOLOGICAL UNIVERSITY

DELHI

(BATCH: 2013-2016)

DECLARATION

I hereby state that the work which is being presented in the thesis report entitled **STEP UP IN IMAGE DEHAZING USING WAVELET DECOMPOSITION & GUIDED FILTERS** by **Harpreet Kaur** in partial fulfillment of requirements for the award of degree of **Master of Technology in Signal Processing and Digital Design** submitted at **Department of Electronics and Communication Engineering, Delhi Technological University, Delhi** is an authentic record of my own work. The matter presented in this thesis report has not been submitted by me in any other University / Institute for the award of Master of Technology degree.

Harpreet Kaur
Enrollment No.: 2K13/SPD/25

July, 2016

DELHI TECHNOLOGICAL UNIVERSITY

CERTIFICATE

This is to certify that the thesis entitled **STEP UP IN IMAGE DEHAZING USING WAVELET DECOMPOSITION & GUIDED FILTERS** submitted by **Harpreet Kaur**, enrollment number **2K13/SPD/25** at **Department of Electronics and Communication Engineering, Delhi Technological University, Delhi** for partial fulfillment of requirements for the award of degree of **Master of Technology in Signal Processing and Digital Design** has been carried out by her under my supervision.

Dr. Sudipta Majumdar
Assistant Professor
Department of Electronics and Communication Engineering
Delhi Technology University
New Delhi - 110042

July, 2016

ACKNOWLEDGEMENT

I would like to express my gratitude to my supervisor Dr. Sudipta Majumdar for the useful comments, remarks and engagement through the learning process of this master thesis.

Furthermore I would like to thank Mr. Rajesh Rohilla and our Head of Department, Mr. Prem R. Chaddha for the support on the way.

Also, I like to thank Chiranjeev Singh (IIM-A grad.), for sharing his pearls of wisdom with us during the course of this research. I would like to thank my loved ones, who have supported me throughout entire process.

ABSTRACT

In the present work, haze removal of images based on dark channel prior approach has been proposed. Based on the observation that haze impacts low frequency component of the image, only approximate part of the hazy image extracted using lifting DB4 wavelet is processed by proposed dark channel prior algorithm. Haze imaging model along with dark channel prior has been used to estimate atmospheric light and transmission. Patch size used for determining dark channel has been made adaptive on the basis of image size. Besides, airlight is obtained from larger patch to ensure more accurate estimation in the presence of localized light sources. Further, transmission has been estimated separately for each of the three color channels considering the phenomena that different color channels undergo different scattering in the atmosphere depending upon their wavelengths. In addition to this, transmission of near white objects has been selectively increased to prevent them from getting over saturated. Further, fast guided filter has been employed to refine transmission map in place of soft matting. Results show that the proposed method gives better performance as image contrast, entropy and SSIM have increased and runtime cost has been significantly decreased. Problem of bluishness observed in classical method also has been reduced.

CONTENTS

CHAPTER 1

INTRODUCTION

Haze is an environmental occurrence that does not only adversely affect the visual quality of an image for human perception but also many machine vision applications whose performance greatly depends on the quality of the underlying image. Thereby, the requirement for removal of haze becomes obligatory. But doing this very much needed task is not an easy job as haze thickness depends on an unknown parameter ‘depth’. Trying to retrieve depth information from a single input image is highly under constrained problem. So, initially haze removal from multiple images or with any other supplementary information became popular. However, in most of the real scenarios, it is practically impossible to obtain multiple images of a scene and this allowed single image haze removal to become widespread. Single image dehazing being under constrained, works on some estimations or priori knowledge to perform the task. More the correctness of estimations better will be the quality and fidelity of the haze free image.

In recent times, single image haze removal based on Dark Channel Prior, proposed by He et al. [1] has become quite prevalent being realistic, less complicated and efficient in haze removal. Many researches have been proposed based on this prior to further improve and optimize the algorithm for different imaging conditions.

Dark Channel Prior is centered on the thought that in most of the outdoor clear images, there exists at least one color in RGB color space that will be nearly zero in a window. That means, one can find many clear colored objects. As it suggests, it won't hold true for sky regions or whitish objects e.g. white structures or cars. In addition, He's [1] method becomes time consuming due to refinement based on soft matting.

In this thesis, we put forward a methodology, partially inspired from some of the previously developed techniques in order to optimize the DCP based method to be more suitable for practical real time applications without compromising on image fidelity. We apply lifting Daubechies (db4) wavelet decomposition merged with Fast Guided filtering [2] to ensure faster operation. To deal with the issue of blue horizon and to preserve the natural colors of the image, we calculate transmission of the medium for each color channel separately. We also apply adaptive transmission correction factor to solve the near white scene problem and hybrid adaptive patch size to solve the problem of localized light sources.

1.1 Thesis Summary

The thesis report is structured as follows. In chapter 2, haze imaging equation is discussed, around which revolves our complete study. In the later part of this chapter, our broad revision on various single image based dehazing methods related to Dark Channel Prior has also been carried out. In chapter 3, various steps of conventional DCP technique developed by He et al. [1] are explained in detail. In chapter 4, we document our study and research work so as to overcome the drawbacks of DCP algorithm and produce high quality haze free image. Our results on images depicting various scenarios are presented in chapter 5. Based on the comparison between our and He's haze free images, we outline both qualitative and quantitative analysis. Chapter 6 summarizes the results and concludes the thesis work. Finally, in chapter 7, we discuss the shortcomings of the algorithm and future scope of the work.

CHAPTER 2

BASICS AND BACKGROUND

This chapter discusses Haze Imaging equation. The equation forms the ground for our thesis and has been used widely in the onward content.

Later in this chapter, former works in context of single image dehazing based on Dark Channel Prior has been asserted. In the course of our discussion, our understanding on the mentioned works based on our evaluation has also been shared.

2.1 Haze Imaging Equation

In 1975, McCartney suggested airlight scattering model [3] which was later elaborated by Narasimhan and Nayar [4]. The haze imaging equation generally utilized as a part of dehazing procedure is:

$$I(x) = t(x)J(x) + A(1 - t(x)) \tag{2.1}$$

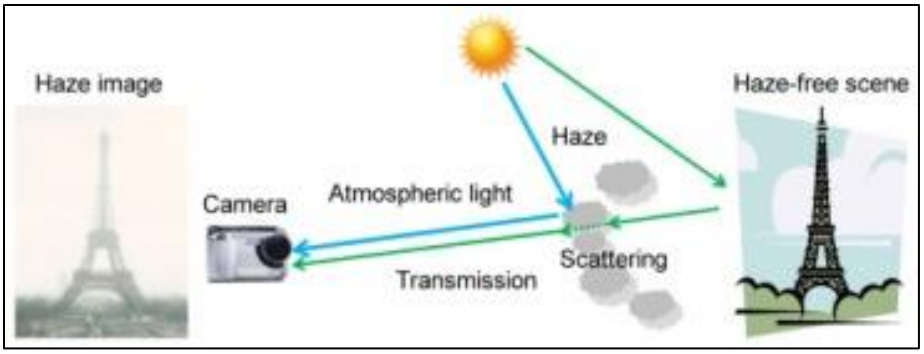

Figure 2.1:Haze Imaging Equation based depiction [5]

where, x is location of the pixel, I is input hazy image, J is haze free image, A is airlight and t is transmission of the medium through which light travels, i.e., air in present case.

The first term 'J(x) t(x)' in equation (2.1) is named as *'direct attenuation'* that denotes the amount of light that reaches the camera straight from the object with the multiplication of attenuation factor caused by medium.

The second term 'A (1 - t(x))' is called *'airlight'* that adds in the radiance as the indirect scattered light coming to the camera. Of course, the reason for scattering is the haze/particles present in the atmosphere that is the target of our exercise.

2.2 Literature Survey

A large number of researches have been done based upon Dark Channel Prior assumption. In the duration of our study, we have evaluated some of those techniques and our conclusions are underneath:

C.H. Hsieh et al. [6] proposed pixel based dark channel, i.e., with patch of size 1x1. This eliminates the need of soft matting. This method works faster however it suffers from halo artifacts.

C.H. Yeh1 et al. [7] introduced an additional bright channel prior to detect regions with minimal haze density. The criterion appears to be false for black objects and shadow regions.

Yogesh et al. [8] simply deployed erosion and dilation for refinement process. The method is confined to a smaller patch size (3x3) beyond which it appears incapable to eliminate halos. Moreover, the moment it achieves halo removal, oversaturation of image emerges as a new problem.

H.Yu Yang et al. [9] used median filter to refine the transmission inherently in the algorithm and adds no extra computation cost.

Y. Yang et al. [10] used discrete Haar wavelet transform and guided filtering [11] to speed up the dehazing algorithm.

Y. Song et al. [12] used pixel wise dark channel or local maximum saturation as guidance image for the guided filtering refinement. This enhanced further the speed of the algorithm since here the guidance images are grey scale in contrast to RGB.

Jiajie Liu et al. [13] optimized transmission by utilizing the difference of image intensity and airlight for every pixel. It performs satisfactorily in sky region however performance is degraded for non-sky images.

Yi-Jui Cheng et al. [14] resolved the localized light sources impact by computing the airlight from dark channel of 45x45 patch.

Dark channel assumption of He [1] fails in sky regions. This leads to inaccurate transmission estimation and oversaturation of sky as the outcome. C. Chengtao et al. [15] performed image segmentation to two regions: sky and non-sky and determine their parameters independent of each other to deal with oversaturation. The method is not very friendly, as it needs user intervention to tune the image dependent threshold value for segmentation.

T. Han and Y. Wan [16] worked on to make transmission estimation more accurate. The value of estimated transmission is varied according to the distance of pixel intensity from airlight. It’s true that this method works well for the sky parts but at the same time leads

to oversaturation of the rest of image. It is quite tedious to tune the above method so as to find parameters that fits in and works well for both sky and non-sky image parts.

Xipan Lu et al. [17] worked on this problem by proposing a compensation term in transmission computation that considered sky region.

C. Yang and F. Liu [18] resolved the near white object problem in initial DCP [1] inspired by underwater dehazing [19]. They increased the transmission with an additive term which is based on the logic of deviation of difference of max. and min. pixel color channel intensity to the average of this quantity.

Many techniques based on pixel wise dark channel prior calculation avoid time-consuming refinement process to eliminate halo and blocky artifacts; however this leads to wrong estimation of atmospheric light when some white objects or structures are present in the image. Secondly, since dark channel of such objects is not dark, it leads to underestimated transmission. In both such scenarios, oversaturation of haze free images occurs.

Another case of over saturation occurs when white objects are present in near scenes of the image. In this case also, dark channel is also dark leading to underestimation of transmission. He et al. [1] stated this as ‘white marble problem’ in his paper.

In our present work, we put forward a methodology somewhat obtained from the above stated works, to develop an optimized algorithm based on DCP which ensures fast and accurate dehazing results. A very efficient wavelet decomposition, Lifting scheme with Daubechies (Db4) has been deployed. Transmission estimation has been optimized to solve the ‘white marble problem’. Adaptive patch size has been used to deal with localized light sources in the images. Refinement process has been performed with fast guided filtering [2] technique. Further, problem of bluishness in conventional DCP [1] has been dealt with by processing the three color channels separately.

CHAPTER 3

CONVENTIONAL DARK CHANNEL PRIOR BASED APPROACH

With due reference to haze imaging equation (2.1) familiarized in former chapter, our aim is to determine scene radiance J from input hazy image I. Intuitively, for this, we need to estimate airlight A and transmission t.

In this chapter, we discuss in detail the Dark Channel Prior based dehazing technique [1].

3.1 Dark Channel Prior

Image dehazing is an under constrained problem with impracticability of multiple images of same scene under different conditions. To solve this with single image, some prior or assumptions are needed.

Tan [20] assumed that the contrast of the hazy image is lesser than the haze free image. His method provide high contrast results however at times, it becomes incapable of faithfully recovering images due to oversaturation.

Fattal [21] considered the statistical independent nature of luminance and transmission. His method works well but is limited to low haze density.

Dark Channel Prior assumption of He et al. [1] is based on the observation that for most of the outdoor haze-free images (except sky), there exists at least one color channel out of RGB color space which has intensity value tending to zero in a patch. We may simply validate this assumption from images underneath:

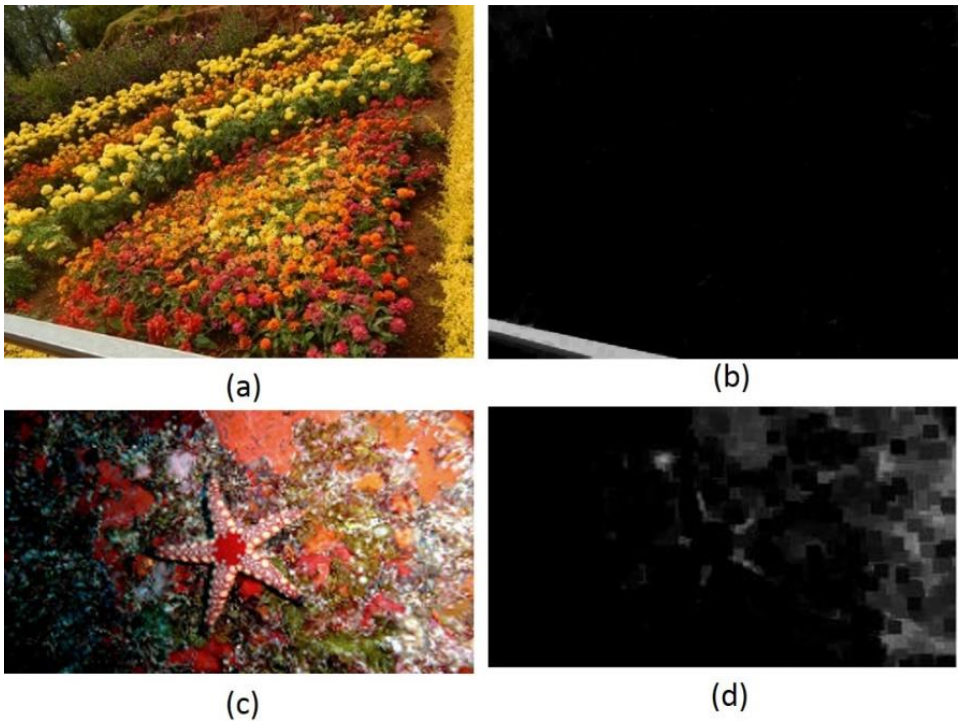

Figure 3.1: (a, c) Outdoor clear images; (b, d) respective dark channel with 15x15 patch

As the logic suggests, it is the presence of colorful objects, shadow areas, irregular structures etc. in many real world images leading to validity of this prior in most of the cases. Exception to this is sky regions and near white structures.

In contrast to the above observation for clear images, dark channel for haze free images is not too dark. An intuitive reason for this is the presence of haze that brightens the pixels.

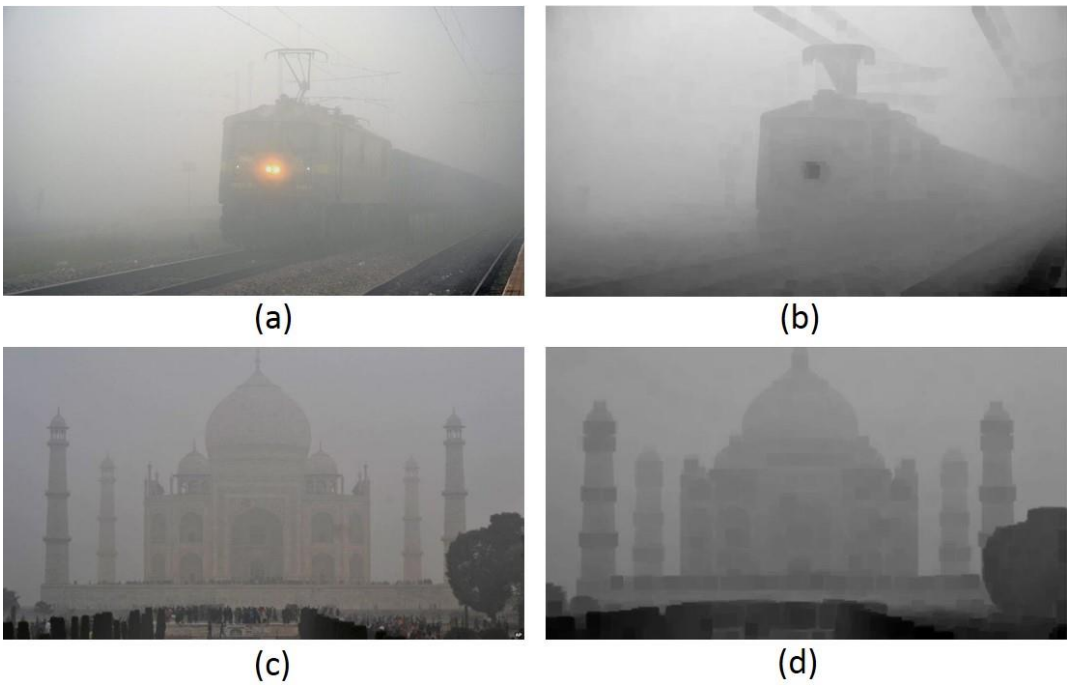

Figure 3.2: (a, c) Hazy images; (b, d) respective dark channel with 15x15 patch

He's[1] Dark Channel Prior algorithm is depicted in the following flow diagram:

Figure 3.3: Flow Diagram for DCP Algorithm

3.1.1 Dark Channel Computation

Dark channel is calculated with two minimum operations as follows:

$$I^{dark}(x) = \min_{y \in \Omega(x)} \left(\min_{c \in \{R,G,B\}} I^c(y) \right) \tag{3.1}$$

where, c refers to the color channel in the RGB color space and Ω refers to the patch or window considered for dark channel computation.

3.1.2 Airlight Estimation

To estimate airlight, average intensity of pixels in hazy image corresponding to 0.1% of the pixels in the dark channel having highest intensity values is calculated. This airlight is assumed to be constant for the whole image but different for three color channels – Red, Green and Blue. Defining in this manner takes care that white objects present in the image like white cars, buildings etc. may not be mistakenly chosen to estimate airlight.

3.1.3 Transmission Estimation

To calculate transmission, rewriting equation (2.1) as:

$$\frac{I^c(x)}{A^c} = t(x)\frac{J^c(x)}{A^c} + 1 - t(x) \tag{3.2}$$

Calculating dark channel on both sides of the above equation, we get,

$$\min_{y\in\Omega(x)}\left(\min_c \frac{I^c(x)}{A^c}\right) = \tilde{t}(x)\min_{y\in\Omega(x)}\left(\min_c\left(\frac{J^c(x)}{A^c} + (1 - t(x)\right)\right) \tag{3.3}$$

Here, $\tilde{t}(x)$ is transmission which is assumed to be constant in a patch. Now, since dark channel corresponding to a haze free image tends to zero:

$$J^{dark}(x) = \min_{y\in\Omega(x)}(\min_c J^c(y)) = 0 \tag{3.4}$$

That is,

$$\min_{y\in\Omega(x)}\left(\min_c \frac{J^c(x)}{A^c}\right) = 0 \tag{3.5}$$

From equation (3.5) and (3.3), we get,

$$\tilde{t}(x) = 1 - \min_{y \in \Omega(x)} \left(\min_{c} \frac{I^c(x)}{A^c} \right) \tag{3.6}$$

3.1.4 Transmission Refinement Using Guided Filter [11]

In earlier research work, He et al. [1] proposed the use of soft matting technique developed by A. Levin [22] to refine transmission so as to deal with halo artifacts. Though effective, this technique is the major contributor to the increase in running time of the dehazing algorithm. To overcome this shortcoming and enable the algorithm for real time applications, He et al. [1] developed an edge aware filtering technique - 'Guided Filter' to replace soft matting.

Replacing soft matting by guided filtering dramatically increased the speed of the algorithm without compromising the quality of the output image.

3.1.4.1 Introduction to Guided Filter

Guided filter constitutes filtering of an input image 'p' on the basis of a guidance image 'I'. It assumes that there exists a linear relationship between the guidance and the output image 'q' as depicted by the equation below:

$$q_i = a_k I_i + b_k, \forall_i \in \omega_k \tag{3.7}$$

where (a_k, b_k) are linear coefficients calculated from the input and guidance image. These linear coefficients are assumed to be constant in a window 'ω_k' of radius 'r'. This nearby direct model guarantees that q has an edge just in the event that I has an edge, in light of the fact that:

$$q_i = a_k I_i + b_k, \forall_i \in \omega_k \tag{3.8}$$

To find the value of (a_k, b_k), following cost function is minimized in window ω_k:

$$E(a_k, b_k) = \sum_{i \in \omega_k} ((a_k I_i + b_k - p_i)^2 + \varepsilon\, {a_k}^2) \tag{3.9}$$

where 'ε' is regularization parameter. Solution of equation (3.9) is given by:

$$a_k = \frac{\frac{1}{|\omega|}\sum_{i \in \omega_k} I_i p_i - \mu_k \overline{p_k}}{\sigma_k^2 + \varepsilon} \tag{3.10}$$

and

$$b_k = \overline{p_k} - a_k \mu_k \tag{3.11}$$

where, μ_k is the mean and σ_k^2 is the variance of guidance image 'I' and; $|\omega|$ are the number of pixels in window 'ω_k'. For example, the mean of 'p' in window ω_k is given by:

$$\overline{p_k} = \frac{1}{|\omega|} \sum_{i \in \omega_k} p_i \tag{3.12}$$

Filtering output q_i can be computed from equation (3.8).

In any case, a pixel i is included in all the covering windows ω_k that spreads over i. So the estimation of q_i in (3.8) is not unique when it is processed in various windows. A straightforward method is to average out all the conceivable estimations of q_i. So subsequent to figuring (a_k, b_k) for all windows ω_k in the image, filtering output is computed by:

$$q_i = \frac{1}{|\omega|} \sum_{k | i \in w_k} (\, a_k I_i + b_k) \tag{3.13}$$

Equation (3.13) can be rewritten as:

$$q_i = \overline{a_\iota} I_i + \overline{b_\iota} \tag{3.14}$$

Where $\overline{a_\iota}$ and $\overline{b_\iota}$ are the average coefficients of all windows covering i.

Yet, as ($\bar{a}_i$, $\bar{b}_i$) are the output of a mean filter, their slopes can be relied upon to be much smaller than that of I close solid edges. In this circumstance, we can in any case have $\nabla q \approx \bar{a}\nabla I$, implying that abrupt intensity changes in I can be protected in q.

3.1.4.2 Guided Filter Working Principle

Referring back to equation (3.8), (3.10) and (3.11) and assuming that $I \equiv p$, we get,

$$a_k = \sigma_k^2/(\sigma_k^2 + \varepsilon) \tag{3.15}$$

And

$$b_k = (1 - a_k)\mu_k \tag{3.16}$$

Following two cases can be observed:

Case 1: *Edge region – Region of high variance*

Here, we have $\sigma_k^2 >> \varepsilon$, so $a_k \approx 1$ and $b_k \approx 0$. Therefore, output image $q = I$ (guidance image). Thus, patches having high variance will be preserved, i.e. edges present in the guidance image will remain unaltered.

Case 2: Flat region – Region of low variance

Here, we have $\sigma_k^2 << \varepsilon$, so $a_k \approx 0$ and $b_k \approx \mu_k$. Therefore, output image $q = \mu_k$ (mean of pixels in window ω_k). Thus, flat patches i.e. regions with low variance will be smoothed out.

3.1.4.3 Guided Filter Algorithm

"Input: radius r, regularization ε, input image p, guidance image I

Output: filtering output q

1. $mean_I = f_{mean}(I)$

   $mean_p = f_{mean}(p)$

   $corr_I = f_{mean}(I .* I)$

   $corr_{Ip} = f_{mean}(I .* p)$

2. $var_I = corr_I - mean_I .* mean_I$

   $cov_{Ip=} corr_{Ip} - mean_I .* mean_I$

3. $a = cov_{Ip} ./ (var_I + \varepsilon)$

   $b = mean_p - a .* mean_I$

4. $mean_a = f_{mean}(a)$

   $mean_b = f_{mean}(b)$

5. $q = mean_a .* I + mean_b$"

3.1.4.4 Guided Filter Applications

Though guided filter was developed as edge preserving smoothing filter, it can be used in diverse applications depending on the value of 'r', 'ε' and guidance image 'I'. In this subsection, we discuss some of the applications of guided filter.

1) *Smoothing Filter:* To employ guided filter as smoothing filter, we may take guidance image ≡ filtering input image. Smaller value of ε and higher value of radius r gives more smoothing effect. For illustration, consider the figure below:

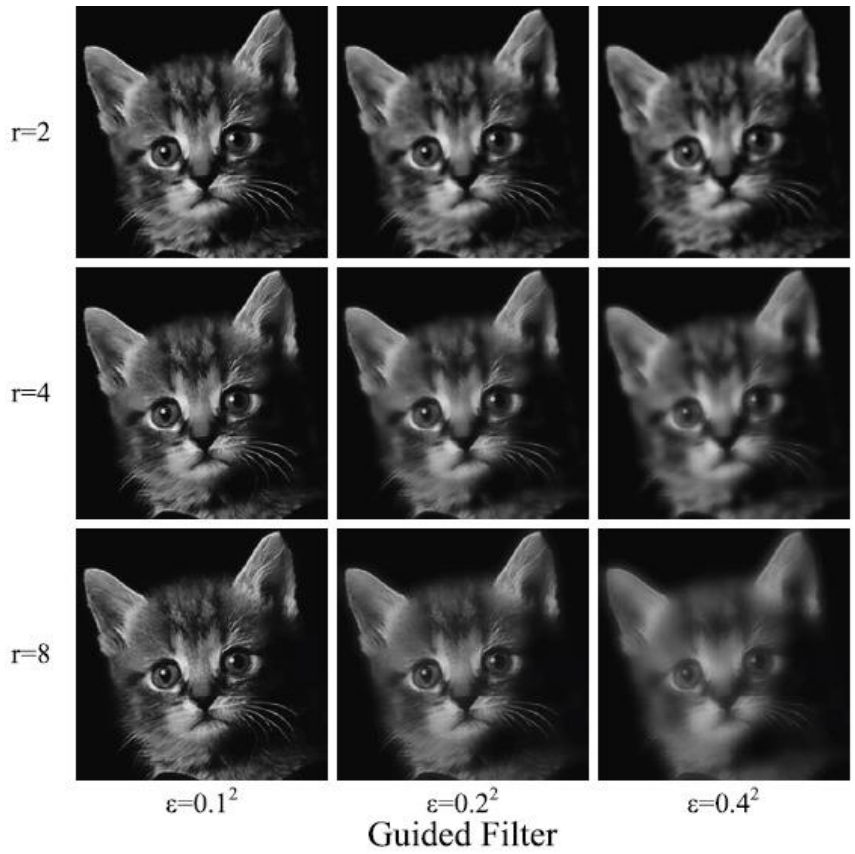

Figure 3.4: Guided filter as smoothing filter

2) *Flash / No Flash Denoising*: In [27], a no-flash image is denoised under the guidance of its flashed image. Figure below demonstrates this:

Figure 3.5: Guided filter used for flash / no-flash denoising

3) Structure Transfer Filtering: Due to linear model, $q = aI + b$, guided filter can be used to transfer structure from guidance image to input image. For illustration, consider the figure below:

Figure 3.6: Guided filter used for structure transferring

This is a very important application of guided filter in view of haze removal applications. This feature of guided filter can be exploited for transferring the original structure of the scene to blocky coarse transmission. This is illustrated in figure 3.7.

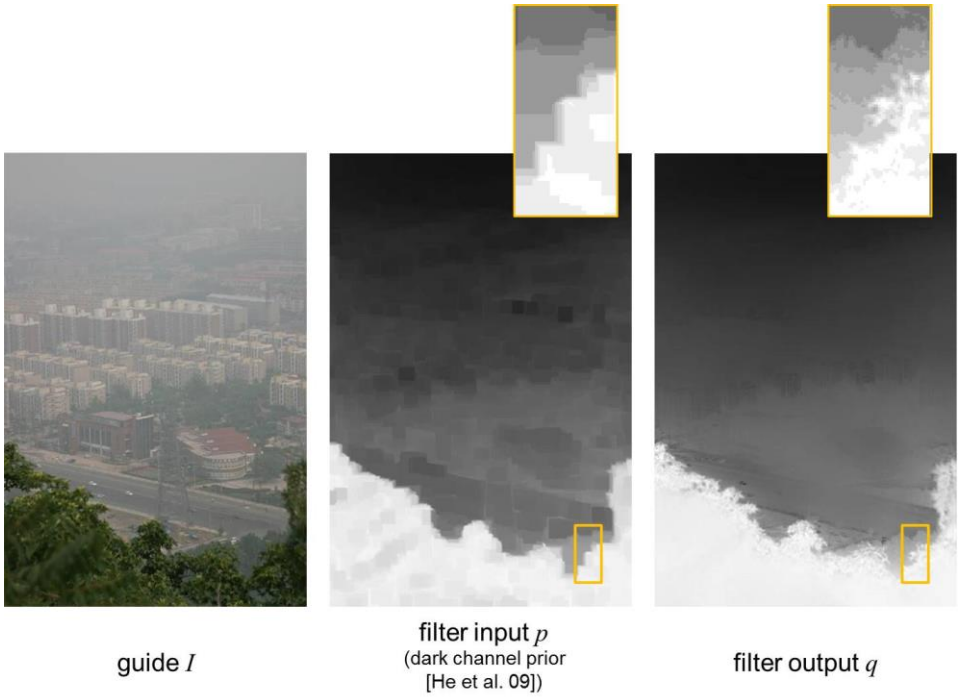

Figure 3.7: Guided filter used for transmission refinement

3.1.5 Scene Radiance Restoration

Having evaluated transmission and air light, scene brilliance can be ascertained using haze imaging equation. If for some pixel transmission value goes too low, correspondingly scene radiance will go very high in each color channel. To stay away

from this circumstance, He et al. [1] limits transmission at 0.1 as lower bound. Numerically,

$$J(x) = \left(\frac{I(x) - A}{max(t(x), t_0)} \right) + A \tag{3.17}$$

CHAPTER 4

PROPOSED SCHEME

In our proposed algorithm, we have attempted to overcome the following shortcomings of He's method:

1. High computation time
2. Incorrect estimation of atmospheric light in the presence of localized light sources
3. Saturation of near white objects
4. Bluishness of scenes near horizon

4.1 Step Up Using Wavelet Decomposition

Since haze is a low frequency phenomenon, we simply process the low frequency part of the picture as opposed to the entire picture. This lessens the run time of dehazing calculation.

Y.Yang et al. [10] decomposed image into four components – image approximation, vertical details, horizontal details and diagonal details using Haar discrete wavelet transform. The approximation image containing low frequency component is then further processed for image dehazing. This gives the classical DCP algorithm ample speed boost.

4.1.1 Proposed Method

We employ Db4 wavelet (Db2 in matlab), implemented using lifting scheme, to obtain approximation image containing low frequency information for further processing via haze removal algorithm. Due to involvement of less complex operations as compared to discrete wavelet transform (convolution, up-sampling and down-sampling), our algorithm is faster than He's method [1] and computationally more efficient than Yang's method. Also, since lifting is an in-place algorithm, less memory space is required.

4.1.1.1 The Lifting Scheme

Lifting is a scheme developed by Wim Sweldens [23]-[26] for constructing second-generation wavelets that need not be essentially dilation and translation of any function. To implement any discrete wavelet transform only finite number of lifting steps is needed. Discrete wavelet transform are traditionally implemented using filter banks. Lifting scheme takes advantage of the similarities between high pass and low pass filters to speed up the computation. Lifting starts with a very simple wavelet called Lazy wavelet from which a new wavelet having improved properties is gradually build.

Lifting is prediction and error decomposition of discrete wavelet transform. Approximation or scaling coefficients are predictors for the next stage whereas details or wavelet coefficients are the prediction errors in the current stage.

Lifting scheme can be illustrated by diagram below:

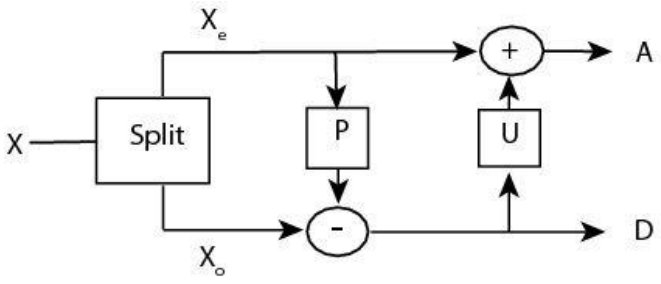

Figure 4.1: Lifting scheme implementation [27]

As shown in the figure, it involves three steps – *Split, Predict and Update*:

1. Split — Divides input signal 'f ' into even and odd polyphase components

$$\text{Even component: } f(2n); \text{ odd component: } f(2n+1) \tag{4.1}$$

2. Predict (also dual lifting) — Predicts odd components from neighboring even components with predictor operation 'P' and with details (high pass) as prediction error.

$$d(n) = f(2n+1) - P(f(2n)) \tag{4.2}$$

Odd components are then retrieved as

$$f(2n+1) = P(x(2n)) + d(n) \tag{4.3}$$

3. Update (also primal lifting): Updates the even samples with an update operator 'U' applied to detail sequence, This produces approximation (low pass) wavelet components 's'.

$$s(n) = f(2n) + U(d(n)) = (f(2n) + f(2n+1))/2 \tag{4.4}$$

4.1.1.2 Decomposition of DB4 into Lifting

Daubechies DB4 transform has 4 filter coefficients:

Low pass

$$h_0 = \frac{1+\sqrt{3}}{4\sqrt{2}} \quad h_1 = \frac{3+\sqrt{3}}{4\sqrt{2}} \quad h_2 = \frac{3-\sqrt{3}}{4\sqrt{2}} \quad h_3 = \frac{1-\sqrt{3}}{4\sqrt{2}} \tag{4.5}$$

High pass

$$g_0 = h_3 = \frac{1-\sqrt{3}}{4\sqrt{2}} \quad g_1 = -h_2 = -\frac{3-\sqrt{3}}{4\sqrt{2}}$$
$$g_2 = h_1 = \frac{3+\sqrt{3}}{4\sqrt{2}} \quad g_3 = -h_0 = \frac{1+\sqrt{3}}{4\sqrt{2}} \tag{4.6}$$

Using filter coefficients in equations A.25 to A.30 in appendix,

$$P(z) = \begin{bmatrix} h_e(z) & h_o(z) \\ g_e(z) & g_o(z) \end{bmatrix}$$
$$= \begin{bmatrix} 1 & \sqrt{3} \\ 0 & 1 \end{bmatrix} \begin{bmatrix} \frac{\sqrt{3}}{4} + \frac{\sqrt{3}-2}{4} z^{-1} & 0 \\ 0 & 1 \end{bmatrix} \begin{bmatrix} 1 & z \\ 0 & 1 \end{bmatrix} \begin{bmatrix} \frac{\sqrt{3}+1}{\sqrt{2}} & 0 \\ 0 & \frac{\sqrt{3}-1}{\sqrt{2}} \end{bmatrix} \tag{4.7}$$

Approximate and detail coefficients can be obtained from the relation:

$$\begin{bmatrix} \lambda(z) \\ \gamma(z) \end{bmatrix} = P(z)^{-1} \begin{bmatrix} f_e(z) \\ z^{-1} f_o(z) \end{bmatrix} \tag{A.17}$$

where

$$P(z)^{-1} = \begin{bmatrix} \frac{\sqrt{3}-1}{\sqrt{2}} & 0 \\ 0 & \frac{\sqrt{3}+1}{\sqrt{2}} \end{bmatrix} \begin{bmatrix} 1 & -z \\ 0 & 1 \end{bmatrix} \begin{bmatrix} \frac{\sqrt{3}}{4} + \frac{\sqrt{3}-2}{4} z^{-1} & 0 \\ 0 & 1 \end{bmatrix} \begin{bmatrix} 1 & -\sqrt{3} \\ 0 & 1 \end{bmatrix} \tag{4.8}$$

Above decomposition can be summarized as:

Forward wavelet transform:

1) Split $$\lambda_{-1,k} \leftarrow f(2k) \; and \; \gamma_{-1,k} \leftarrow f(2k+1) \tag{4.9}$$

2) Update1 $$\lambda_{-1,k} \leftarrow \lambda_{-1,k} + \sqrt{3}\,\gamma_{-1,k} \tag{4.10}$$

3) Predict $$\gamma_{-1,k} \leftarrow \gamma_{-1,k} - \frac{\sqrt{3}}{4}\lambda_{-1,k} - \frac{\sqrt{3}-2}{4}\lambda_{-1,k-1} \tag{4.11}$$

4) Update2 $$\lambda_{-1,k} \leftarrow \lambda_{-1,k} - \gamma_{-1,k+1} \tag{4.12}$$

5) Normalize $$\lambda_{-1,k} \leftarrow \frac{\sqrt{3}-1}{\sqrt{2}}\lambda_{-1,k} \; and \; \gamma_{-1,k} \leftarrow \frac{\sqrt{3}+1}{\sqrt{2}}\gamma_{-1,k} \tag{4.13}$$

Inverse wavelet transform:

1) Undo Normalize $$\lambda_{-1,k} \leftarrow \frac{\sqrt{3}+1}{\sqrt{2}}\lambda_{-1,k} \; and \; \gamma_{-1,k} \leftarrow \frac{\sqrt{3}-1}{\sqrt{2}}\gamma_{-1,k} \tag{4.14}$$

2) Undo Update2 $$\lambda_{-1,k} \leftarrow \lambda_{-1,k} + \gamma_{-1,k+1} \tag{4.15}$$

3) Undo Predict $$\gamma_{-1,k} \leftarrow \gamma_{-1,k} + \frac{\sqrt{3}}{4}\lambda_{-1,k} + \frac{\sqrt{3}-2}{4}\lambda_{-1,k-1} \tag{4.16}$$

4) Undo Update1 $$\lambda_{-1,k} \leftarrow \lambda_{-1,k} - \sqrt{3}\,\gamma_{-1,k} \tag{4.17}$$

Lifting has numerous advantages as listed below:

- It is faster with number of flops reduced by a factor of two.
- It is an in place algorithm, therefore it requires less memory
- Using lifting it is easy to build integer to integer transform.

- Constructing wavelets using lifting does not require prior knowledge of Fourier transform
- Any lifting transform is immediately reversible, simply by changing + with – and vice versa

Figure 4.2 and 4.3 shows the hazy image and its corresponding wavelet decomposition components.

4.2 Dark Channel Prior

The formula for computing dark channel, as discussed in Chapter 3 is:

$$I^{dark}(x) = \min_{y \in \Omega(x)} \left(\min_{c \in \{R,G,B\}} I^c(y) \right) \tag{3.1}$$

Dark channel of hazy image is shown in figure 4.4.

Figure 4.2 (a): Input hazy image

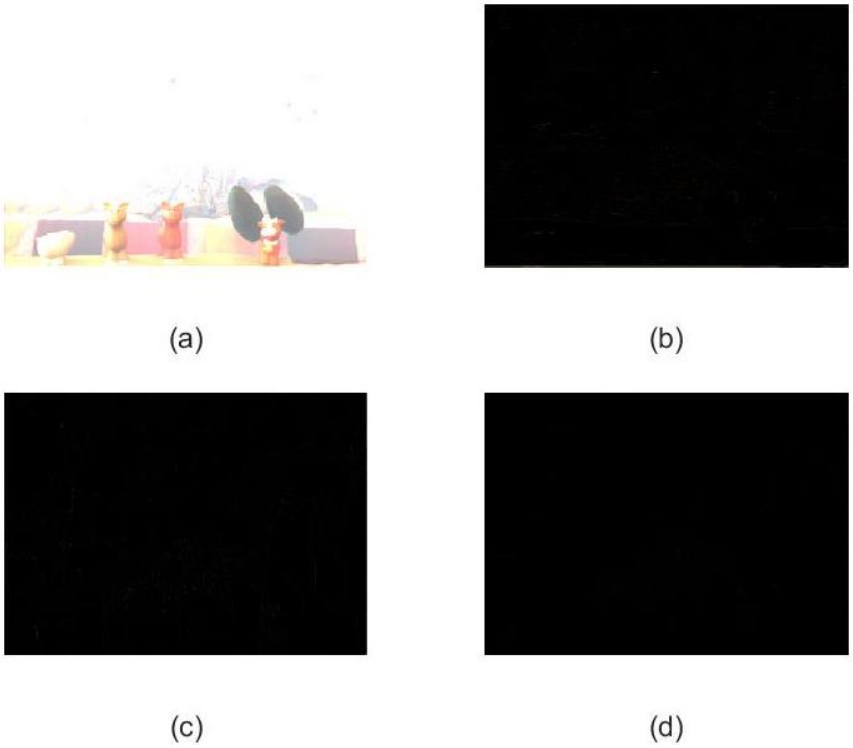

Figure 4.3 (b): Wavelet components (a) CA: Approximation (b) CH: Horizontal (c) CV: Vertical (d) CD: Diagonal

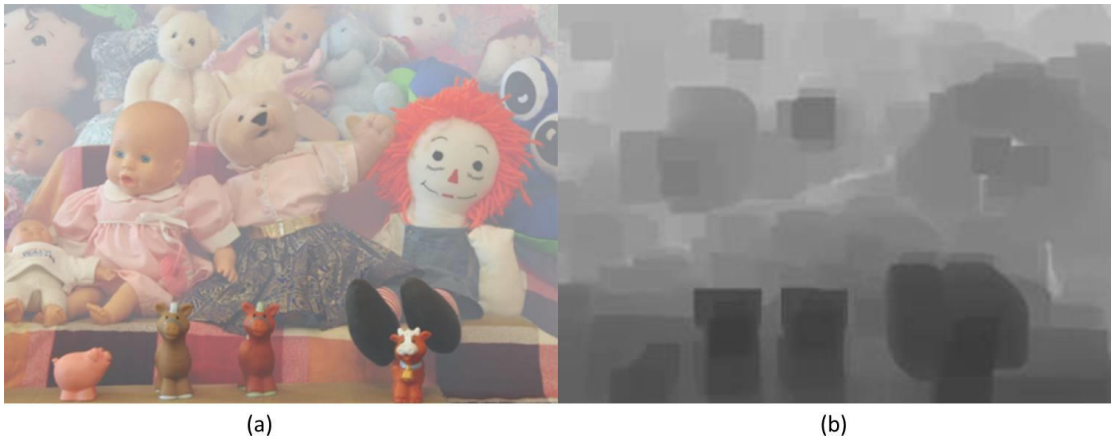

Figure 4.4: (a) Input hazy image (b) Dark channel using 15x15 patch

4.2.1 Impact of Patch Size

When using smaller patch size with respect to size of image, the possibility of obtaining a pixel out of RGB color space with intensity tending to zero decreases. In such case, transmission computation (equation 3.5) becomes less accurate. Vice versa for large patch sizes, transmission computation is more accurate. However, opting for larger patch

size leads to stronger halo and blocky artifact. It is still possible to deal with these artifacts with the help of various refinement techniques. Figure below illustrates the impact of various patch sizes. Note that when patch size is bigger than required, some haze is left in the image.

Figure 4.5: Recovering images using different patch sizes (a) Input hazy images (b) Using 3 × 3 patches (c) Using 15 × 15 patches (d) Using 30 × 30 patches [1]

In our work, we have ascertained dynamic patch size to guarantee that it is sufficiently big, consequently encouraging accurate measurement of transmission.

4.3 Estimating Atmospheric Light

While estimating airlight, He considered a patch size of 15x15. This size can take care of small white objects but is not big enough to take care of localized light sources. So, in the presence of such localized light sources, atmospheric light is calculated using pixels from wrong position, i.e., pixels near the center of the light source. To deal with this problem, Yi-Jui Cheng et al. [14] proposed estimating atmospheric light using dark channel computed for patch of size 45 x 45. Method works well as 45 x 45 patch is big enough to hide light sources as big as street lights, car headlights etc., in the dark channel of the image. The result published in their research work is shown in figure 4.6.

In our work, we have used hybrid patch size, i.e. different patch size for estimating atmosphere and different patch size for estimating transmission. We have kept the patch size for calculating atmosphere larger than the patch size for estimating transmission. The patch size chosen for estimating atmospheric light is not fixed to 45x45, rather it is decided dynamically from the size of the image. We have proposed this change so as to ensure that localized light sources are never mistakenly chosen for estimating airlight irrespective of their sizes.

4.4 Estimating Transmission

Firstly, He's method suffered from the problem of saturation for near white scenes. This happens because when dark channel of near white large objects is computed, it does not comes out dark because of high intensity in all the three color channels. Due to this, the near white object is considered as a far object by the algorithm, underestimating the transmission which in turn leads to over estimation of scene radiance i.e. saturation.

Feng Liu et al. [18] effectively dealt with the above mentioned issue by increasing transmission of those pixels for which difference between the highest and lowest intensity levels is nearly the same as the average of difference in the image.

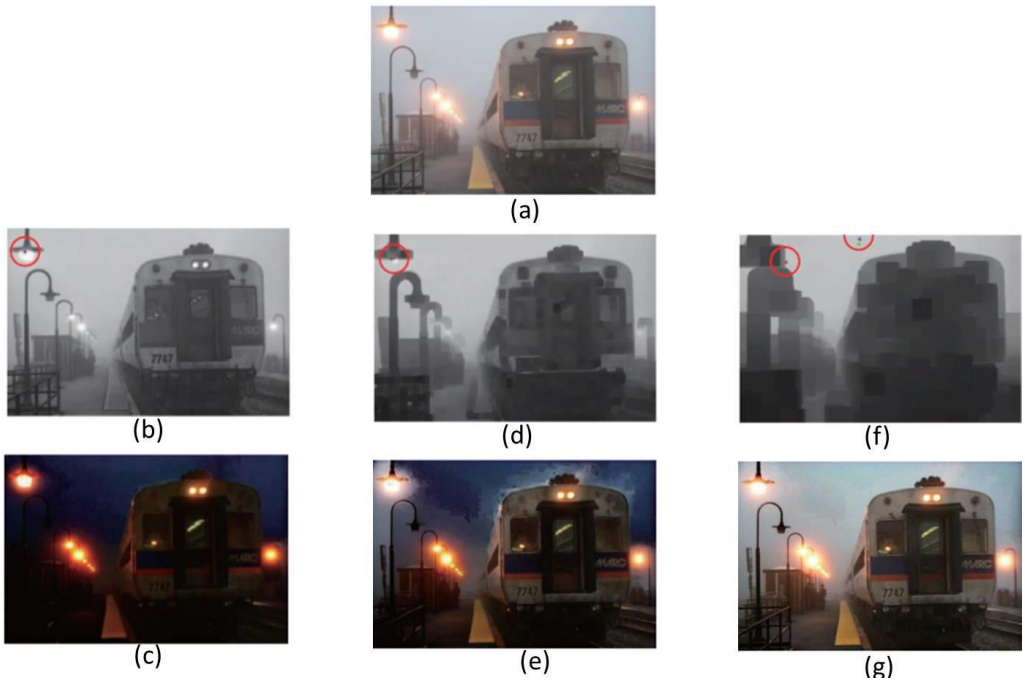

Figure 4.6: (a) Input hazy Image (b) 3x3 Dark channel (c) Recovered image using 3x3 patch (d) 15x15 Dark Channel (e) Recovered image using 15x15 patch (f) 45x45 Dark Channel (g) Recovered image using 45x45 patch [14]

Figure 4.7: (a) Input image (b) Result of He's method [1] (c) Result of Feng's method [18]

Note that the temple behind in the figure above has been lost by the proposed technique.

With tunable parameters set as proposed in their research work: γ=2 and uplim=0.14, Feng's method yielded impressive results for images having majorly near white scenes but in other case it seems as if the haze is not completely removed. In our project, we have used Feng's method but with a little change so as to avoid saturation while removing maximum amount of haze at the same time.

Secondly, He's conventional DCP method undergoes blue horizon problem, i.e., objects near the horizon appears blue. This happens so because transmission is kept constant among color channel, but in actual it depends on color. So, to overcome this issue, in our work, we have proposed to compute transmission separately for each channel [8]. The equation for transmission estimation in our case gets modified as follows:

$$\tilde{t^c}(x) = 1 - \min_{y \in \Omega(x)} \left(\frac{I^c(x)}{A^c} \right) \tag{4.18}$$

Only one minimum operator is required as calculated for each color separately.

4.5 Refinement Using Fast Guided Filter

Replacement of soft matting by guided filter made conventional DCP algorithm very fast. To further increase the speed of guided filter, He [2] proposed to subsample the input and guidance image, perform filtering process using these subsampled images and at last up sample the final output. This increases the speed drastically when compared to soft matting technique. The numerical values found after experimentation are listed in the Result section.

In our work, we apply fast guided filter to speed up the dehazing algorithm.

In the next subsection, we discuss in detail the cause of halo artifacts for which we need to go for refinement techniques.

4.5.1 Dealing with Halo Artifacts

Halos appear in the areas of depth discontinuities occurring in a patch. Since, transmission estimation is patch based, these different depth areas are wrongly determined. In this process, over estimation of transmission for far located regions lead to halos.

We apply fast guided filtering to remove these halo artifacts in our haze removal process. Figure (4.8) depicts the coarse and refined transmission using proposed method.

4.6 Calculating Scene Radiance

Once atmospheric light and refined transmission are obtained, we can simply use these parameters in haze imaging equation to retrieve scene radiance.

$$J(x) = \left(\frac{I(x) - A}{max(t(x), t_0)} \right) + A \tag{3.17}$$

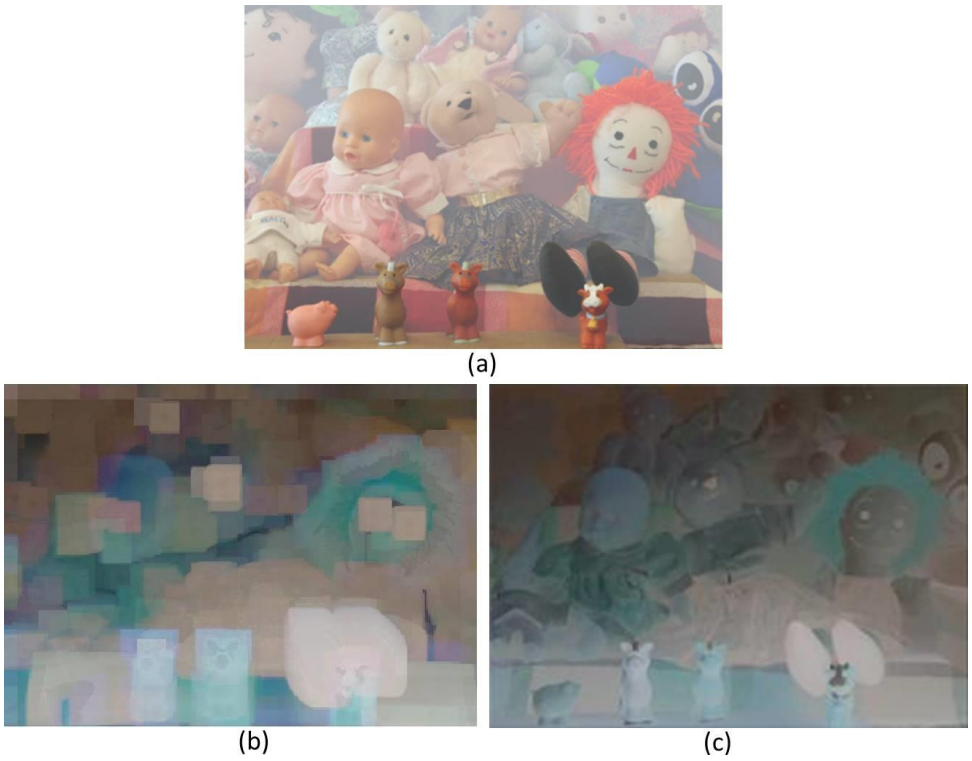

Figure 4.8: (a) Hazy image (b) Coarse transmission (c) Refined transmission

4.7 Proposed Algorithm

The algorithm of our end to end work is depicted by the block diagram below. In another block diagram that follows, the dehazing algorithm has been presented..

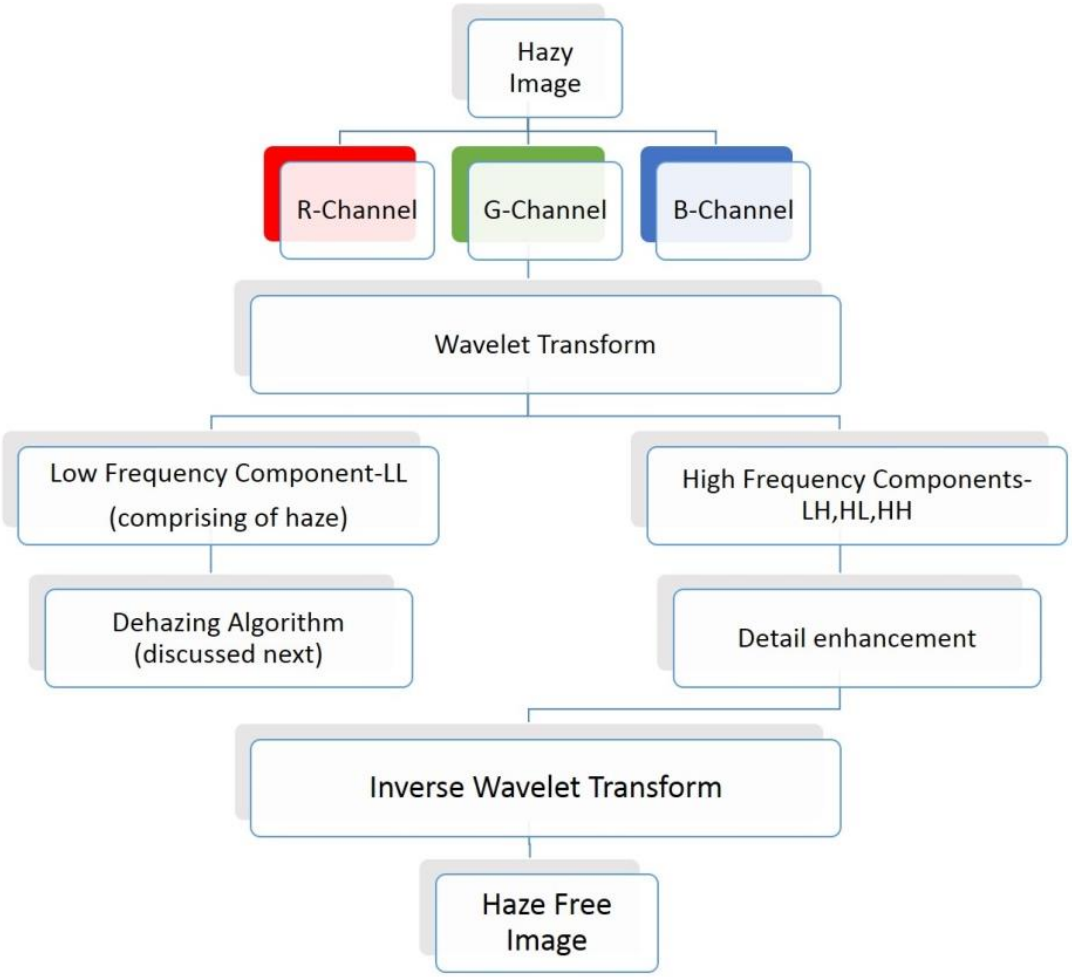

Figure 4.9(a): Block diagram of our approach

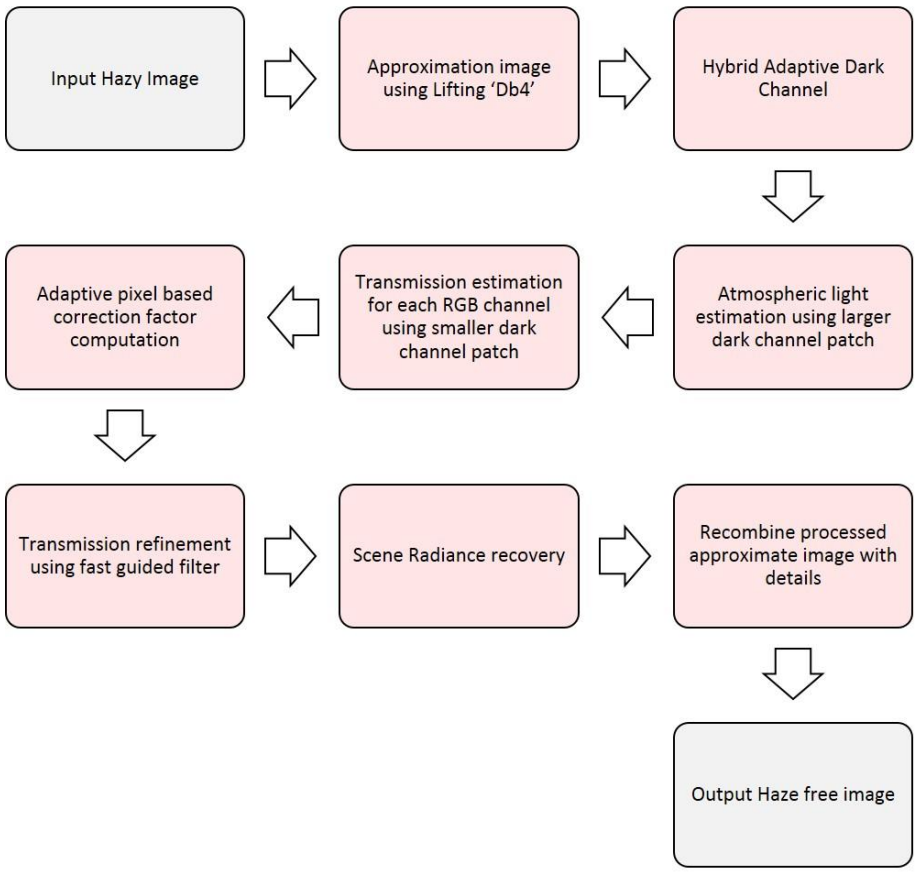

Figure 4.6(b): Block diagram (II) of our dehazing algorith

CHAPTER 5

SIMULATION AND RESULTS

Based on our proposed algorithm in chapter 4, here we discuss and compare the results so obtained with outputs from conventional method. We have done quantitative and qualitative examination on the results based on the entropy, structural similarity to the input hazy image and contrast.

Simulation platform used for experimentation is Matlab-R2012a, Windows 10 Home 64-bit, Intel core-i3 1.90 GHz (Quad core), and 4096 MB RAM.

5.1 Qualitative Investigation

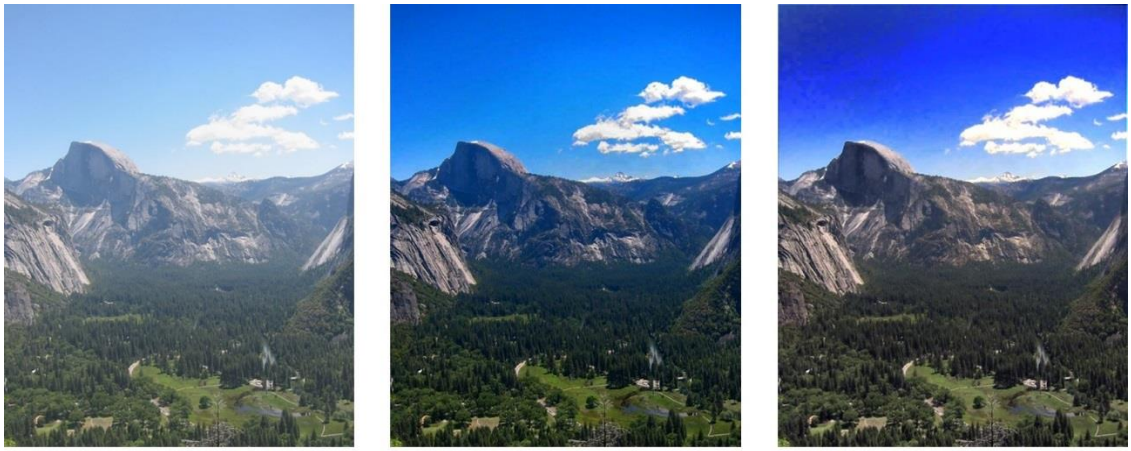

Figure 5.1: Blue Horizon Problem (a) Input hazy image (b) He's output. Mountains near horizon turn blue (c) Our output. Original color of mountains remains intact.

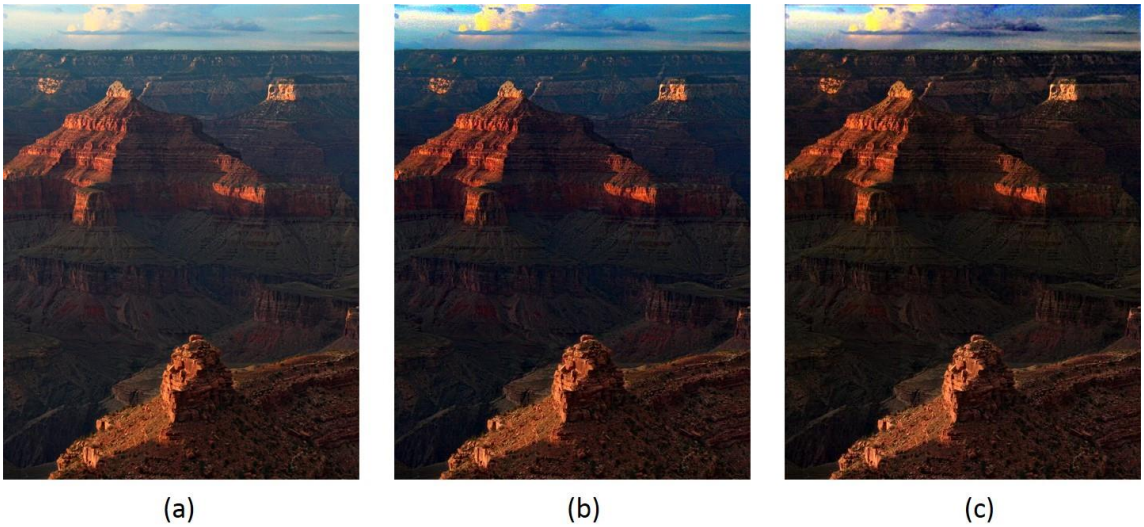

Figure 5.2: Blue Horizon Problem (a) Input hazy Image (b) He's output. Canyons near horizon turn blue (c) Our output. Original color of canyons remains intact.

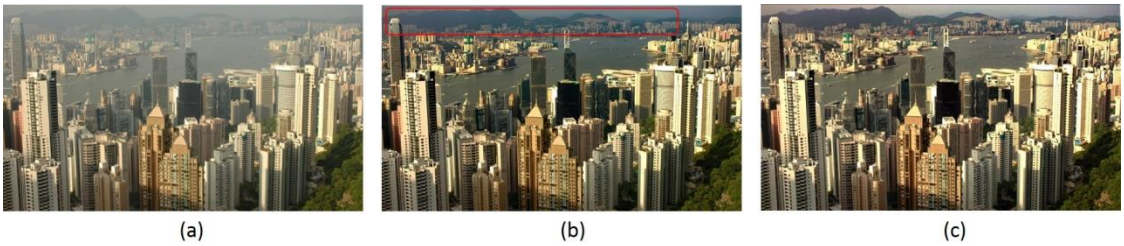

Figure 5.3: Blue Horizon Problem (a) Input hazy image (b) He's output. Mountains near horizon are not clear (c) Our output. Mountains near horizon are clear and don't turn blue.

Figure 5.4: Blue Horizon Problem (a) Input hazy image (b) He's output (c) Our output

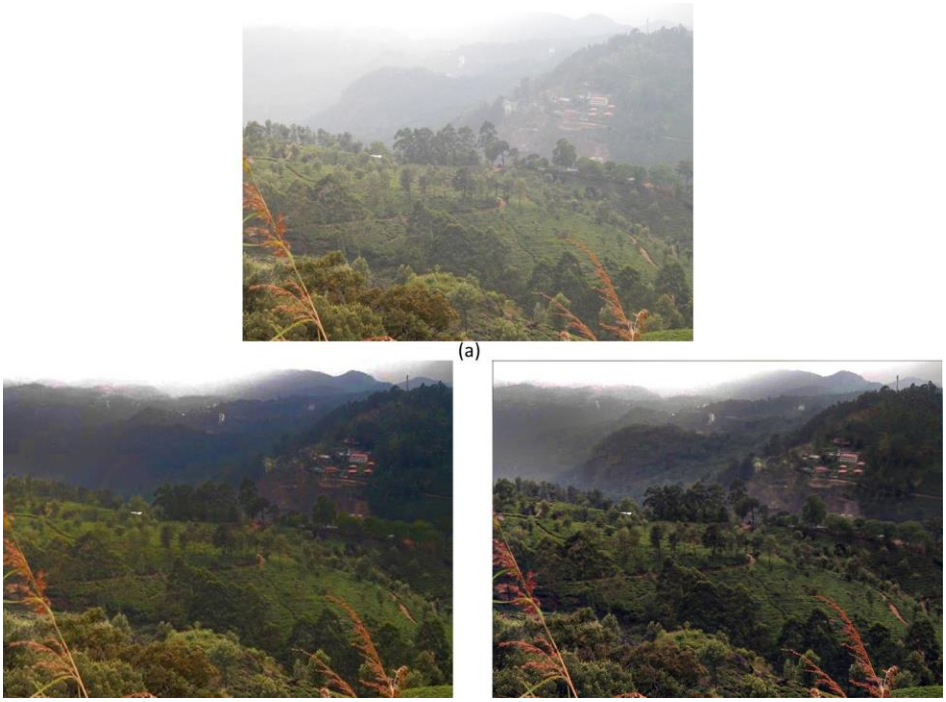

Figure 5.5: Blue Horizon Problem (a) Input hazy image (b) He's output (c) Our output

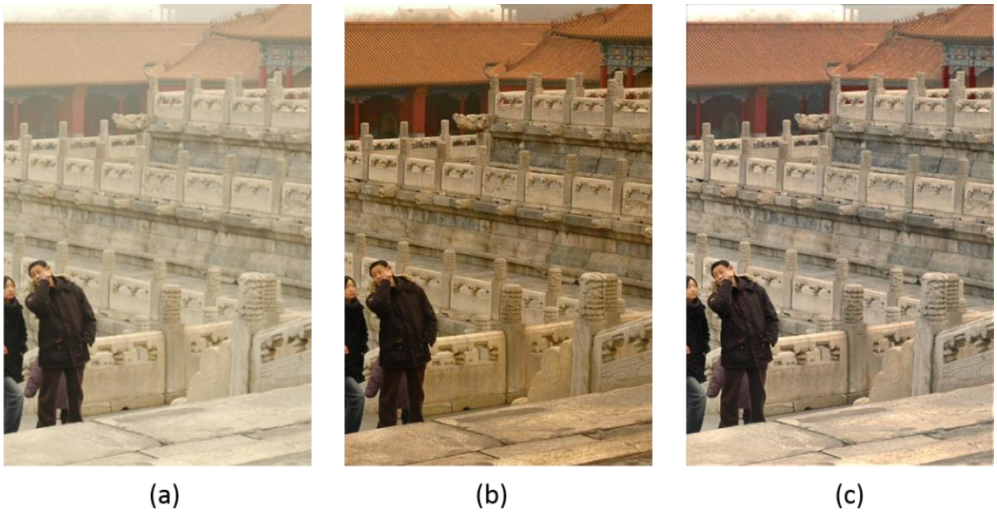

Figure 5.6: Near white scene saturation (a) Input hazy image (b) He's output. Marble is saturated (c) Our output. Color of marble remains intact.

(a) (b) (c)

Figure 5.7: Saturation (a) Input hazy image (b) He's output. Cones are saturated (c) Our output. Color of cones remains intact.

In figure 5.1, the mountains turn bluish near horizon when conventional DCP [1] is used for dehazing. As discussed before, this happens due to keeping transmission uniform over the three color channel – Red, Green and Blue, when in actual transmission is color dependent. Our method solves this problem as we calculate transmission separately for each color channel. Same can be observed for the next three figures - (5.2), (5.3), (5.4) and (5.5).

In figure 5.6, transmission of marble is under estimated in He's algorithm [1]. Due to which it appears saturated or say yellowish in the final haze free image. To deal with problem, we introduce a correction factor to increase transmission in such regions. Our result shows that the problem of saturation of near white scenes has been successfully dealt with.

In figure 5.7, He's method results in over saturation i.e. the natural color of cones is lost. On the other hand, our method successfully dehaze the image without compromising at color fidelity.

5.2 Quantitative Investigation

We use entropy, SSIM and RMS contrast to compare image quality results as described underneath:

- **Entropy**: It is a measure of randomness. It can characterize image texture. Images having lot of sky region, very low contrast or large number of pixels with similar

value have low entropy. Low entropy value characterizes homogeneous regions. Thus hazy images, which have haze spread throughout, have low values of entropy as compared to haze free images. Mathematically,

$$Entropy\ H = -\sum_{i} p_i(log_2 p_i) \tag{5.1}$$

where, p is the histogram count.

Entropy comparison shown below in table 5.1 proves that our algorithm performs better compared to classical DCP method.

- **Structural Similarity Index (SSIM)**: It measures image degradation due to processing like image dehazing in present case. This metric requires reference image. Mathematically,

$$SSIM(x, y) = \frac{(2\mu_x\mu_y + c_1)(2\sigma_{xy} + c_2)}{(\mu_x^2 + \mu_y^2 + c_1)(\sigma_x^2 + \sigma_y^2 + c_2)} \tag{5.2}$$

where, μ_x is the mean of x, μ_y is the mean of y, σ_x^2 is the variance of x, σ_y^2 is the variance of y, σ_{xy} is the variance of y, c_1 and c_2 are variables to stabilize division.

In present work, we use input hazy image as the reference image. Higher value of SSIM indicates that structure information is well maintained in the haze free image

- **Root Mean Square Contrast**: It is same as the standard deviation of pixel intensities from the average intensity in a grey scale image. More contrast means better distinguishability among different objects in an image. Mathematically,

$$RMS\ Contrast = \sqrt{\frac{1}{MN}\sum_{i=0}^{N-1}\sum_{j=0}^{M-1}\left(I_{ij} - \bar{I}\right)^2} \tag{5.3}$$

For grayscale image of size MxN, having average intensity $\bar{I}$ and intensities normalized to a range of [0,1].

Analysis in the table 5.1 below shows that results produced from our method has better contrast than He's method.

Table 1: Entropy, SSIM and Contrast comparison

Parameter	*Entropy*			*SSIM*		*Contrast*		
Image	**Hazy input**	**He's Method**	**Proposed method**	**He's Method**	**Proposed Method**	**Hazy input**	**He's Method**	**Proposed method**
Figure 5.1	7.58	7.62	7.19	0.69	0.63	8.06	7.16	8.31
Figure 5.2	6.73	6.63	6.43	0.63	0.64	7.19	6.21	6.48
Figure 5.3	7.56	7.64	7.74	0.79	0.78	7.54	9.25	9.92
Figure 5.4	7.06	7.39	7.51	0.74	0.70	5.10	6.49	7.15
Figure 5.5	7.56	6.88	7.05	0.65	0.63	8.37	8.07	8.90
Figure 5.6	7.35	7.66	7.72	0.81	0.81	6.59	6.75	7.53
Figure 5.7	7.22	7.06	7.17	0.68	0.69	5.54	4.40	5.75

Next, **Execution Time Comparison** of our algorithm compared to conventional DCP with fast guided filtering is shown in the table below

Table 2: Algorithm execution time

Figure	Image Size	DCP with FGF	Proposed Scheme
Figure 5.1	588x742	6.865s	4.910s
Figure 5.2	450x600	4.401s	3.095s
Figure 5.3	800x457	5.940s	4.050s
Figure 5.4	800x431	5.495s	3.784s
Figure 5.5	1152x864	14.460s	9.161s
Figure 5.6	400x600	3.981s	2.771s
Figure 5.7	465x384	3.030s	2.173s

CHAPTER 6

DISCUSSION AND CONCLUSION

In this thesis, we studied in detail the prevalent dehazing algorithm – Dark Channel Prior proposed by He et al. [1]. We analyzed thoroughly the limitations and cases where the algorithm fails. Based on our extensive study of various recent research works in this context, we propose a novel optimum method to address some of the problematic areas like speed, blue horizon problem, localized light sources and saturation of near white scenes. Our result shows the effectiveness of our method in above stated parameters.

Speed is taken care of by employing lifting wavelet scheme for Daubechies 4 wavelet and subsampling technique in guided filter. We solve the problem of blue horizon by computing transmission for each color channel separately. We do not allow localized light sources to put an impact on our computation of airlight by ensuring big enough patch size. Also, to remove haze to the fullest, while of course retaining the natural feeling of scene depth, we use smaller patch size to estimate transmission than used for estimating atmospheric light. Thus, in one line we employ adaptive hybrid patch size scheme. Lastly, we effectively solve the problem of near white scene saturation is tackled using adaptive correction factor for transmission.

CHAPTER 7

FUTURE WORK

The proposed algorithm assumes constant value of atmospheric light, which is non-uniform over image in reality. Due to this, we still face over exposure issue in sky region. For example, consider the image below:

Figure 7.1: (a) input hazy image, (b) saturated dehazed image

To develop a dehazing algorithm that works well even for sky region will be our goal in future.

REFERENCES

1. Kaiming He, Jian Sun, and Xiaoou Tang, Fellow IEEE, "Single Image Haze Removal Using Dark Channel Prior", *IEEE Transactions on Pattern Analysis and Machine Intelligence*, vol. 33, no. 12, December 2011
2. Kaiming He, Jian Sun, "Fast Guided filter", *Microsoft.com*, arXiv:1505.00996v1(cs.CV), 5 May 2015
3. McCartney and Earl J., "Optics of the Atmosphere: Scattering by Molecules and Particles", New York, *John Wiley and Sons*, Inc., 1976. 421 p. 1 (1976)
4. S. Narasimhan and S. Nayar, "Vision and the Atmosphere," *International Journal on Computer Vision*, vol. 48, no. 3, Jul 2002, pp. 233–254
5. www.osapublishing.org
6. Cheng-Hsiung Hsieh, Yu-Sheng Lin and Chih-Hui Chang, "Haze Removal Without Transmission Map Refinement Based On Dual Dark Channels", *IEEE International Conference on Machine Learning and Cybernetics*, vol. 2, July 2014
7. Chia-Hung Yeh, Li-Wei Kang, Cheng-Yang Lin and Chih-Yang Lin, "Efficient Image/Video Dehazing through Haze Density Analysis Based on Pixel-based Dark Channel Prior", *IEEE Conference on Information Security and Intelligence Control (ISIC)*, August 2012
8. Yogesh Kumar, Jimmy Gautam, Ashutosh Gupta, Bhavin V. Kakani and Himansu Chaudhary, "Single Image Dehazing Using Improved Dark Channel

Prior", IEEE conference on Signal Processing and Integrated Networks (SPIN), February 2015

9. Hung-Yu Yang, Pei-Yin Chen, Chien-Chuan Huang, Ya-Zhu Zhuang, Yeu-Horng Shiau, "Low Complexity Underwater Image Enhancement Based on Dark Channel Prior", *IEEE Conference on Innovations in Bio-inspired Computing and Applications (IBICA)*, December 2011
10. Yanjing Yang, Zhizhong Fu, Xinyu Li, Chang Shu and Xiaofeng Li, "A Novel Single Image Dehazing Method" , *IEEE International Conference on Computational Problem-solving (ICCP)*, October 2013
11. K. He, J. Sun, and X. Tang., "Guided image filtering", Proceedings of European Conference on Computer Vision (ECCV)
12. Yingchao Song, Haibo Luo, Bing Hui and Zheng Chang, "An Improved Image Dehazing and Enhancing Method Using Dark Channel Prior", *IEEE Chinese Control and Decision Conference (CCDC)*, May 2015
13. Jiajie Liu, Jieying Zheng, Ziguan Cui, Guijin Tang and Feng Liu, "An Improved Image Dehazing Algorithm Based on Dark Channel Prior", *IEEE Workshop on Advanced Research and Technology in Industry Applications (WARTIA)*, September 2014
14. Yi-Jui Cheng, Bo-Hao Chen, Shih-Chia Huang, Sy-Yen Kuo, Andrey Kopylov, Oleg Seredin, Leonid Mestetskiy, Boris Vishnyakov, Yury Vizilter, Oleg Vygolov, Chia-Ruei Lian and Chi-Ting Wu, "Visibility Enhancement of Single Hazy Images Using Hybrid Dark Channel Prior", *IEEE International Conference on Systems, Man, and Cybernetics*, October 2013
15. C. Chengtao, Z. Qiuyu and L. Yanhua, "Improved Dark Channel Prior Dehazing Approach Using Adaptive Factor", *IEEE International Conference on Mechatronics and Automation (ICMA)*, August 2015
16. Ting Han and Yi Wan, "A Fast Dark Channel Prior-based Depth Map Approximation Method for Dehazing Single Images", IEEE Third International Conference on Information Science and Technology, March 2013

17. Xipan Lu, Guoyun Lv and Tao Lei, “Fast Single Image Dehazing Algorithm”, *IEEE Conference on Audio, Language and Image Processing (ICALIP)*, July 2014
18. Feng Liu and Canmei Yang, “A Fast Method for Single Image Dehazing Using Dark Channel Prior”, *IEEE International Conference on Signal Processing, Communications and Computing (ICSPCC)*, August 2014
19. Nicholas Carlevaris-Bianco, Anush Mohan and Ryan M. Eustice, “Initial Results in Underwater Single Image Dehazing”, *IEEE Oceans Mts*, September 2010
20. Robby T. Tan, “Visibility in Bad Weather from a Single Image”, *IEEE Computer Vision and Pattern Recognition*, 2008
21. Fattal, R., “Single Image Dehazing”, *ACM Transactions on Graphics*, 27(3), 721-729
22. Anat Levin, Dani Lischinski and Yair Weiss, “A Closed-Form Solution to Natural Image Matting”, *IEEE Transactions on Pattern Analysis and Machine Intelligence*, vol.30, no. 2, pp. 228-242, February 2008
23. W. Sweldens, "The Lifting Scheme: A Construction of second generation wavelets," SIAMJ. Math. Anal 1997
24. W. Sweldens, "The Lifting Scheme: A Custom Design construction of Biorthogonal," Wavelets Appl. Comput. Harmon. Anal. 3(2); 1996
25. I. Daubechies and W. Sweldens "Factoring wavelet transform into lifting steps" Technical report, Bell Laboratories, Lucent Technologies, 1996
26. W. Sweldens “Wavelets and the lifting scheme: A 5 minute tour“, ZAMM - Journal of Applied Mathematics and Mechanics, vol. 76 (Suppl. 2), pp. 41-44, 1996

APPENDIX A

Lifting Scheme Decomposition Steps

For a discrete data sequence $f(k)$, z transform is:

$$f(z) = \sum_{k} f(k) z^{-k} \tag{A.1}$$

Above equation can be expanded as:

$$f(z) = f(0)z^{0} + f(1)z^{-1} + f(2)z^{-2} + f(3)z^{-3} + \cdots \tag{A.2}$$

And

$$f(-z) = f(0)z^{0} - f(1)z^{-1} + f(2)z^{-2} - f(3)z^{-3} + \cdots \tag{A.3}$$

Upon adding above two equations,

$$\frac{f(z) + f(-z)}{2} = f(0)z^{0} + f(2)z^{-2} + f(4)z^{-4} + \cdots = \sum_{k} f(2k) z^{-2k} \tag{A.4}$$

Now, on down sampling the signal $f(z)$ and keeping only the even values, we get:

$$f_e(z) = \sum_k f(2k) z^{-k} \tag{A.5}$$

Comparing equation (1.4) and (1.5), we get,

$$f_e(z^2) = \frac{f(z) + f(-z)}{2} \tag{A.6}$$

Similarly,

$$f_o(z^2) = \left[\frac{f(z) - f(-z)}{2}\right] z \tag{A.7}$$

Thus, from equation (1.6) and (1.7),

$$f(z) = f_e(z^2) + z^{-1} f_o(z^2) \tag{A.8}$$

Decomposing $f(z)$ using LPF say $h(z)$ and HPF say $g(z)$, i.e.,

$$lp(z) = f(z)h(z) \tag{A.9}$$

And

$$hp(z) = f(z)g(z) \tag{A.10}$$

Above two equations can be written in matrix form as:

$$\begin{bmatrix} lp(z) \\ hp(z) \end{bmatrix} = \begin{bmatrix} h(z) \\ g(z) \end{bmatrix} f(z) \tag{A.11}$$

Down sampling step corresponds to

$$LP(z^2) = lp_e(z^2) = \frac{lp(z) + lp(-z)}{2} = \frac{h(z)f(z) + h(-z)f(-z)}{2} \tag{A.12}$$

And

$$HP(z^2) = hp_e(z^2) = \frac{hp(z) + hp(-z)}{2} = \frac{g(z)f(z) + g(-z)f(-z)}{2} \tag{A.13}$$

Equation (1.12) and (1.13) can be written in matrix form as:

$$\begin{bmatrix} LP(z^2) \\ HP(z^2) \end{bmatrix} = \begin{bmatrix} lp_e(z^2) \\ hp_e(z^2) \end{bmatrix} = \frac{1}{2}\begin{bmatrix} h(-z) & h(z) \\ g(-z) & g(z) \end{bmatrix}\begin{bmatrix} f(-z) \\ f(z) \end{bmatrix} \tag{A.14}$$

In this case, since subsampling is done after calculating all coefficients, it is inefficient. Thus, to increase efficiency down sampling is performed before filtering (considering their even part only), yielding:

$$lp_e(z) = [h(z)f(z)]_e = h_e(z)f_e(z) + z^{-1}h_o(z)f_o(z) \tag{A.15}$$

In the same way,

$$hp_e(z) = [g(z)f(z)]_e = g_e(z)f_e(z) + z^{-1}g_o(z)f_o(z) \tag{A.16}$$

Suppose output of down sampler followed by LPF be $\lambda(z)$, and output of down sampler followed by HPF be $\gamma(z)$. Then, equation (1.15) and (1.16) in matrix form can be written as:

$$\begin{bmatrix}\lambda(z)\\ \gamma(z)\end{bmatrix} = P(z)\begin{bmatrix}f_e(z)\\ z^{-1}f_o(z)\end{bmatrix} \tag{A.17}$$

$P(z)$ is poly-phase matrix given by:

$$P(z) = \begin{bmatrix}h_e(z) & h_o(z)\\ g_e(z) & g_o(z)\end{bmatrix} \tag{A.18}$$

For perfect reconstruction, the LPF $h(z)$ and HPF $g(z)$ need to be complimentary yielding unity determinant of poly-phase matrix. This implies that,

$$P(z) = \begin{bmatrix}1 & 0\\ 0 & 1\end{bmatrix} \tag{A.19}$$

h^{new} is derived from g using primal lifting or update as:

$$h^{new} = h(z) + s(z^2)g(z) \tag{A.20}$$

Similarly, $g^{new}$is derived from h using dual lifting or predict as:

$$g^{new} = g(z) + t(z^2)h(z) \tag{A.21}$$

In polyphase representation equation (1.20) and (1.21) can be written as:

$$P^{new}(z) = \begin{bmatrix} h_e^{new}(z) & h_o^{new}(z) \\ g_e(z) & g_o(z) \end{bmatrix} = \begin{bmatrix} 1 & s(z) \\ 0 & 1 \end{bmatrix} \begin{bmatrix} h_e(z) & h_o(z) \\ g_e(z) & g_o(z) \end{bmatrix} \quad \text{(A.22)}$$

And

$$P^{new}(z) = \begin{bmatrix} h_e(z) & h_o(z) \\ g_e^{new}(z) & g_o^{new}(z) \end{bmatrix} = \begin{bmatrix} 1 & 0 \\ t(z) & 1 \end{bmatrix} \begin{bmatrix} h_e(z) & h_o(z) \\ g_e(z) & g_o(z) \end{bmatrix} \quad \text{(A.23)}$$

Poly-phase matrix can be factorized into finite product upper and lower triangular matrices as:

$$P(z) = \begin{bmatrix} K1 & 0 \\ 0 & K2 \end{bmatrix} \prod_{i=m}^{1} \begin{bmatrix} 1 & s_i(z) \\ 0 & 1 \end{bmatrix} \begin{bmatrix} 1 & 0 \\ t_i(z) & 1 \end{bmatrix} \quad \text{(A.24)}$$

Now, $s_i \; and \; t_i$ can be obtained by writing poly-phase matrix as:

$$P(z) = \begin{bmatrix} h_e(z) & h_o(z) \\ g_e(z) & g_o(z) \end{bmatrix} = \begin{bmatrix} h_e(z) & h_o^{new}(z) \\ g_e(z) & g_o^{new}(z) \end{bmatrix} \begin{bmatrix} 1 & s(z) \\ 0 & 1 \end{bmatrix} \quad \text{(A.25)}$$

This implies that,

$$h_o(z) = s(z)h_e(z) + h_o^{new}(z) \quad \text{(A.26)}$$

And

$$g_o(z) = s(z)g_e(z) + g_o^{new}(z) \quad \text{(A.27)}$$

Similarly,

$$P(z) = \begin{bmatrix} h_e(z) & h_o(z) \\ g_e(z) & g_o(z) \end{bmatrix} = \begin{bmatrix} h_e^{new}(z) & h_o(z) \\ g_e^{new}(z) & g_o(z) \end{bmatrix} \begin{bmatrix} 1 & 0 \\ t(z) & 1 \end{bmatrix} \quad \text{(A.28)}$$

That is,

$$h_e(z) = h_e^{new}(z) + t(z)h_o(z) \quad \text{(A.29)}$$

And

$$g_e(z) = g_e^{new}(z) + s(z)g_o(z) \quad \text{(A.30)}$$